

## Influence of Surfactants and Charges on CdSe Quantum Dots

Ping Yang · Sergei Tretiak · Sergei Ivanov

Received: 13 April 2011 / Published online: 22 July 2011  
© Springer Science+Business Media, LLC 2011

**Abstract** Surface effects significantly influence the functionality of semiconductor nanocrystals. High quality nanocrystals can be achieved with good control of surface passivation by various hydrophobic ligands. In this work, the chemistry between CdSe quantum dots and common surface capping ligands is investigated using density functional theory (DFT). We discuss the electronic structures and optical properties of small CdSe clusters controlled by their size of particle, self-organization, capping ligands, and positive charges. The chosen model ligands reproduce good structural and energetic description of the interactions between the ligands and quantum dots. In order to capture the chemical nature and energetics of the interactions between the capping ligands and CdSe quantum dots, we found that  $\text{PMe}_3$  is needed to adequately model trioctylphosphine (TOP),  $\text{NH}_3$  is sufficient for amines, while  $\text{OPH}_2\text{Me}$  could be used to model trioctylphosphine oxide. The relative binding interaction strength between ligands was found to decrease in order  $\text{Cd-O} > \text{Cd-N} > \text{Cd-P}$  with average binding energy per ligand being  $-25$  kcal/mol for  $\text{OPH}_2\text{Me}$ ,  $-20$  kcal/mol for  $\text{NH}_3$  and  $-10$  kcal/mol for  $\text{PMe}_3$ . Charges on studied stoichiometric clusters were found to have a significant effect on their structures, binding energies, and optical properties.

**Keywords** CdSe quantum dots · Surface ligands · Charges · Density functional theory

---

P. Yang (✉)  
Environmental Molecular Sciences Laboratory, Pacific Northwest National Laboratory,  
902 Battelle Boulevard, Richland, WA 99352, USA  
e-mail: ping.yang@pnnl.gov

S. Tretiak · S. Ivanov  
Center for Integrated Nanotechnologies (CINT), Los Alamos National Laboratory, Los Alamos,  
NM 87545, USA

## Introduction

Semiconductor nanoparticles (NCs) are ligand-surfactant-stabilized particles of 1–100 nm in size and can be placed in the range between molecular compounds and single crystals. They have gained vital attention due to their controllable optical and electronic properties by tuning the size, shape, core/shell formation, and surface manipulation [1–3]. In particular, colloidal quantum dots (QDs) have attracted significant interest in diverse fields including solar energy conversion [4–7], nanosensors [8, 9], light-emitting diodes [10–13], and biomedical imaging [14–18] due to their excellent photostability and resistance to photobleaching [19]. The heterogeneous metal chalcogenide quantum dots, such as CdSe, and CdTe, can be synthesized by convenient organometallic methods with high degree of size control. They are composed of a semiconductor core protected from the surrounding medium with a layer of organic molecules [1, 20]. Cadmium and selenium precursors are reacted in a coordinating solvent at high temperature in excess trioctylphosphine oxide (TOPO) or other alternative solvents [2, 21–24]. It has been shown that substantial control of the synthesis and properties of NCs can be achieved by selecting the appropriate ligands in synthesis processes. The organic capping ligands used in the colloidal synthesis have a profound impact on the nanocrystals' shape, size, composition and morphology [25–32]. A crucial step to design biocompatible quantum dots for biological application is to choose appropriate surface ligands with high affinity and selectivity that can target directly to the binding site of the protein of interest [33, 34].

The surface ligands provide an alternative route to modifying the electronic and chemical properties of quantum dots and have attracted significant attention. The types of ligand species are important in quantum dots chemistry through participating in a variety of properties regulations and stabilizations. Surface ligands, such as alkyl phosphonic acids, carboxylic acids, oleic acid, alkylthiols, alkylamines, and/or shells of inorganic materials play a decisive role in stabilizing the NCs in solution by directly interacting with the surface atoms. The choice of ligand, solvent, and reaction conditions can influence the size and morphology, dipole and ionic interactions of the resulting nanocrystals. These achievements are due to the development of surfactant-controlled growth in hot organic solvent, a synthetic approach for CdSe quantum dots was first introduced in 1993 [1]. Following this seminal work, there are now very effective synthetic methods to produce CdSe nanoparticles and most of the recent syntheses of CdSe nanoparticles are variations on the above common theme. These generic hydrophobic ligands usually need to be replaced by specific functional ligands in order to enable specific targeting and complementary optoelectronic functionality [35]. Experimental studies of CdSe quantum dots capped by oxygen-coordinating ligand TOPO using NMR [36], XPS [37], and EXAFS techniques established that the surface Se atoms are not likely to be passivated, and it appears that surface passivation first and foremost occurs via ligand coordination to surface metal atoms. It remains the most significant challenge to fully understand the ligand exchange mechanisms.

These ligands have been proved to have a strong effect on the electronic and optical properties of passivated NCs by changing surface dangling bonds [38–41]. For example, thiols are observed to quench photoluminescence of CdSe

nanocrystals as hole scavengers [38, 41]; and amines can enhance the quantum yield, colloidal stability and biological interactions which makes themselves as important reagents in synthesis [42, 43]. The known determinants of QD PL efficiency include ligand coverage, binding geometries, electronic passivation efficacy, and liability [16, 44]. Additional data shows that if NCs are not properly passivated by ligands, surface selenium atoms are prone to oxidation and removed from nanoparticle leaving a selenium vacancy [45, 46]. Changing the suspension solvent of NCs can modify various surface ligands [47–50]. The synthetic approach has been switched from a conventional mass action to a more chemically driven approach, which is an achievable by using ligands with chemoselective head groups at cadmium chalcogenide NC surfaces [37, 50, 51]. Recent experimental surveys showed extensive evidence that both the type and the quality of surface passivation are very important for such optical properties as, for instance, the optical gain or photoinduced absorption [52–57]. Recently, it has been noticed that the trace impurities in TOPO and HDA plays a key role in manipulating the shape, composition, crystal growth of NCs [22, 58, 59]. More surface chemistry study is expanded to the semiconductor QDs beyond CdSe [60]. The equilibrium constants for solution phase binding of para-substituted aniline molecules were measured recently and the binding strength of ligands were deduced [61–65]. More binding energies were measured in this manner including phosphonic acid and carboxylic acid [66, 67]. It has been reported very recently that surface ligands can control the synthesis of magic-size quantum dots [68–70]. Paralleling these fields, peculiar structure transformation can be induced by surface modifications [26], as evidenced on the equilibrium between the wurtzite and zinc blende polytypes of CdSe nanocrystals, where it has been shown that short-chain phosphonic acids stabilize the zinc blende phase whereas octadecylphosphonic acids stabilize the wurtzite phase [71].

Whilst experimental scientists have pursued studies through spectroscopic techniques to understand the surface structures and properties correlating to various types of surface ligands [36, 37, 53, 72], theoretical scientists studied the geometrical structures and optical properties, as well as the interactions with the passivation ligands, using various methods spanning from semi-empirical to time-dependent first principle techniques [73–80]. In the past decade, there has been achieved great computational and theoretical progress in understanding the unique properties of QDs. However, complete decipher of the interface phenomena of NCs remains hardly scratched. Limited by the computational resource in the early stage, scientists used various approximate methods to mimic the surface effects. Theoretical studies of the unsaturated valences (dangling bonds) on the surface were either left truncated or saturated by pseudo hydrogen [81] or oxygen atoms [40, 82], rather than more realistic surfactants. The precise nature of ligands was unspecified, and each ligand was assumed to supply single  $sp^3$ -hybridized orbital that bonds with the Cd atoms [80]. As a result, the effect of NC surface reconstruction has been partially addressed. For example, based on the simplistic particle-in-a-box approach, the Effective-Mass Approximation model (EMA) and its “ $k \cdot p$ ” generalization fails to encompass the detailed ligand passivation and focuses on the modification of the envelope of electron wave-functions induced by

the confinement only [83]. So far, EMA was only applied to ligand-free QDs and results were found to significantly disagree with experimental values [84]. Other studies have been carried out for ligand-free QDs at semiempirical techniques [85–88] and density functional theory (DFT) utilizing tight-binding approximation [89–91], Local Density Approximation (LDA) or Generalized Gradient Approximation (GGA) models [92–94]. A ligand potential model has been used to simulate the surface passivation [77, 82, 93]. However, the arbitrary magnitude of the potential and of the distance between the ligands and the surface atoms can affect the calculated values of the optical band gaps. The electronic properties of CdSe nanocrystals were found to be sensitive to their environment in a study that simulated the environment using self-consistent reaction field and semiempirical pseudopotential methods [73, 74, 79, 95–97]. Hydrogen atoms, as excellent terminating ligands for organic systems, were used as explicit model ligands in semiempirical pseudopotential in order to saturate dangling bonds [81]. An improved approach was adopted by using oxygen atoms as passivation ligands to surface Cd [98]. Tight-binding theory was employed in studying the electronic and optical properties of passivated and unpassivated CdS nanocrystals and CdS/ZnS core shell nanocrystals [99, 100]. Ligand-like potentials were used to passivate surface dangling bonds to study the dependence between particle size and optical gaps [101]. In another study, the dangling bonds on the surface were removed by shifting the energies of the corresponding hybrid orbitals well above the conduction band edge by about 100 eV [102]. The possibility of surface reorganization by partially saturating Se dangling bonds thus had been neglected in previous theoretical investigations.

More realistic simulations of the surface reconstruction using first principle methods had been published recently including self-healing and ligand effect of CdSe nanocrystals [78–80, 103]. The ligand models and methodology benchmark on smallest cluster with explicit ligands shows that explicit functional head groups of ligands should be used in simulations in order to capture the chemical nature of surface ligands [104]. Very recently, it was reported using explicit ligands for small nanoclusters mixed with hydrogen atom as stabilizing agents using hybrid density functional theory (B3LYP) and time-dependent density functional theory (TD-DFT) for electronic spectra study [105, 106]. With explicit ligand models, quantification of ligand binding energies between different ligands became possible [66, 79, 107–109], as well as more realistic theoretical studies of nanocrystal growth [74, 110], ligand effects and electronic spectra [111–117], and optical properties of magic-size quantum dots [107, 118, 119]. On related broader studies, adsorption of ligands to various bulk crystal planes was also investigated [79, 119, 120]. There are trends that classical molecular dynamics studies between ligands and NCs start merging in [61, 117].

Given the wide potential applications of quantum dots are approaching, a fundamental understanding of interactions between ligands and quantum dots is a subject of continuing and intense investigations [22, 74, 89, 107, 121–124]. The importance of surface ligands for quantum dots, in terms of stabilization, avoiding surface oxidation and aggregation to protect the optoelectronic properties, has been studied in these reports. The structural chemistry at interfaces between ligands and

QDs is yet to be described at atomistic level in a systematic way. Realistic models with full chemical natures of ligands are needed to understand the nature of ligands binding on quantum dots. In this work, we explore the properties of clusters  $\text{Cd}_6\text{Se}_6$  and  $\text{Cd}_{13}\text{Se}_{13}$  for the size dependency of semiconductor quantum dots, based on the previous methodology investigations [104]. We focus on studying the differences in geometry caused by ligand effects, the relative binding strength of various ligands, and the charge effects in the systems. The excited state calculations using TD-DFT were carried out to investigate the effects from ligands on optical properties.

## Computational Methods

### Methodology

We use DFT methods as implemented in Gaussian 03 package [125], to investigate the structural mechanism of ligands binding and the electronic properties of larger quantum dots, such as  $\text{Cd}_6\text{Se}_6$  and  $\text{Cd}_{13}\text{Se}_{13}$ . The previous study showed that the combination of hybrid functional (B3LYP) combined with basis set LANL2DZ provides reasonable description for the chemistry between ligands and CdSe quantum dots with moderate computational expense [104]. To further validate the methods employed for a small cluster  $\text{Cd}_2\text{Se}_2$  to larger structures, GGA functional OPBE was applied for calculations of small cluster  $\text{Cd}_6\text{Se}_6$ . The results also show that B3LYP hybrid functional offers better description of ligands binding energies than GGA in general. In present work, no symmetry constraints were applied during all geometry optimizations performed.

### CdSe Cluster Models

In this work we continue to use the same ligand binding patterns, as found for the minimal cluster  $\text{Cd}_2\text{Se}_2$  [104], on the gradually larger clusters including  $\text{Cd}_6\text{Se}_6$  and  $\text{Cd}_{13}\text{Se}_{13}$ . These two specific clusters are selected to demonstrate the ligands effects, charge effects, and size effects. Moreover, the  $\text{Cd}_6\text{Se}_6$  structure is selected by being one unit cell of wurtzite structure, which is reported to be the bulk structure for crystal and core structure for large quantum dots.  $\text{Cd}_6\text{Se}_6$  will be an extreme case to understand surface reorganization for minimal wurtzite structure, since all atoms are on surface.  $\text{Cd}_{13}\text{Se}_{13}$  is the next larger wurtzite structure with three fused unit cells, among which one of each shares two faces with the other two unit cells. Alternatively  $\text{Cd}_{13}\text{Se}_{13}$  cluster exists in a cage configuration, being the smallest magic-size cluster reported [70, 126]. A recent report using mass spectrometry showed that the cluster  $\text{Cd}_{13}\text{Se}_{13}$  can stably exist as cage structure with 3 four-membered and 10 six-membered rings on the cage of 12 Se and 13 Cd ions with a Se ion inside [127]. As a result, the  $\text{Cd}_{13}\text{Se}_{13}$  cage cluster was included in our study as an alternative geometry for assessing the ligand binding interactions and charge effects. This will be the first example of a testing case to understand how surface reconstructs for wurtzite and cage structures.

The number of ligands bound to  $\text{Cd}_6\text{Se}_6$  is six with one to each cadmium atom, whereas the number of ligands bound to both  $\text{Cd}_{13}\text{Se}_{13}$  geometries (cage and wurtzite) is 10 instead of 13 (see Table 3). In the cage form, there are totally 10 cadmium atoms that could bind with ligands due to unsaturated bonding. The other three cadmium atoms are fully bound to neighbor selenium ions. Therefore, there are no dangling bonds on these three cadmium atoms. A further validation was applied to confirm that additional ligand binding cannot affect these internal cadmium–selenium interactions. We optimized  $\text{Cd}_{13}\text{Se}_{13}$  cluster with 13 capping ligands as initial set up, i.e. every cadmium atom capped by one ligand molecule. The ligand binding to these saturated Cd atoms is not stable since the optimized geometries show that the ligands attached to the saturated Cd atoms disassociate from the cluster. Similarly, there are also 10 unsaturated Cd atoms with dangling bonds in the wurtzite structure and could be capped by surface ligands. As a result, the degree of surface passivation for cluster  $\text{Cd}_{13}\text{Se}_{13}$  is reduced to 76.9% from 100% in the subsequent calculations. The ligand binding energies and calculated energy differences between wurtzite and cage geometries are listed in Table 2.

### Surface Ligand Models

The use of basic ligands for CdSe quantum dots is essential to achieve the chemical stability of the compounds [44, 114]. The electronegativity of ligands can be investigated theoretically by changing the electron donating groups of the ligands. We gradually introduce methyl groups to increase the electronegativity of the coordinating atom phosphor from  $\text{PH}_3$  to  $\text{PH}_2\text{Me}$  to  $\text{PMe}_2$  to  $\text{PMe}_3$ . Ideally,  $\text{PMe}_3$  is best candidate in order to attain the chemical nature of TOP, which is the one of the most common ligands in synthesis of quantum dots. This demonstrates that the basicity of the phosphines bound to cadmium is an important factor influencing the binding energies and relative stability compared to other ligands. We found that  $\text{PMe}_3$  is required in order to gain good accuracy of binding energies of alkylphosphine from investigations for the cluster  $\text{Cd}_2\text{Se}_2$ . In the case of amines, the simple model  $\text{NH}_3$  is sufficiently accurate to represent both geometries and energies. To further verify the validity of these conclusions for larger clusters, we continued testing the models for ligands on the clusters aforementioned to find out the possible simplest ligand model representing realistic compounds with acceptable accuracy. In this paper,  $\text{PH}_3$  and  $\text{PMe}_3$  are the models for TOP while  $\text{NH}_3$  and  $\text{NMe}_3$  are used as representatives for amines.

$\text{OPH}_3$  is an adequate model for TOP oxide as shown in clusters  $\text{Cd}_2\text{Se}_2$  and  $\text{Cd}_6\text{Se}_6$  simulations. But the simulations for cluster  $\text{Cd}_{13}\text{Se}_{13}$  show that strong hydrogen bonding interactions ( $\text{P-H}\cdots\text{O}$ ) occur between ligands and could cause proton transfer. Due to the loss of spatial freedom of ligands and the closer distances between the ligands on the same crystal facet of larger cluster, such as  $\text{Cd}_{13}\text{Se}_{13}$ , it is unlikely to avoid hydrogen-bonding interactions between ligand molecules at high coverage degree. With the increase of cluster size, this phenomenon will become more pronounced because there are more ligand molecules on less curvature surface. These intermolecular interactions among ligands could be avoided in small clusters thanks to big surface curvature and sufficient space for

ligands to be distributed around the cluster. We also study the more realistic models including OPH<sub>3</sub>, OPH<sub>2</sub>Me, OPHMe<sub>2</sub>, OPMe<sub>3</sub> to find the best comprise between the realistic model, electronegativity, and computation cost by gradually adding methyl groups to phosphine oxide.

### Charge Effects

Quantum dots could be partially charged when they are synthesized. These charged dots could have different properties compared to their neutral counterparts. It is not clear how the charges distribute on the clusters. Although intensive research has been done to investigate the relationship between the properties, and type/size of quantum dots [1], investigations of the effects from extra charges are a rising subject for continuing interest. In the previous study we have observed that ligands bind to the charged Cd<sub>2</sub>Se<sub>2</sub> cluster with much larger binding energies and geometric changes compared to the neutral cases [104]. For the same token, we continued the calculations for the clusters Cd<sub>6</sub>Se<sub>6</sub> and Cd<sub>13</sub>Se<sub>13</sub> with two positive charges (+2). Furthermore, Cd<sub>19</sub>Se<sub>20</sub> cluster was studied as a neutral counterpart for charged cluster Cd<sub>19</sub>Se<sub>19</sub> with +2 charges neutralized by a Se ion with -2 charges. Only singlet electronic states are discussed in this work.

### Ligand Binding Energies

The binding energies listed in Tables 3 and 4 are averaged binding energies per ligand molecule ( $\overline{BE}$ ). One of the issues is the variation of the step-wise binding energy from the averaged binding energy ( $\overline{BE}$  vs.  $BE_2$ ). We define

$$\overline{BE} = \frac{1}{n} (E_{\text{Cd}_m\text{Se}_m\text{L}_n} - E_{\text{Cd}_m\text{Se}_m} - nE_L), \quad \text{where } m = 6, n = 6 \text{ or } 9;$$

$$\text{if } m = 13, n = 10;$$

$$BE_2 = E_{\text{Cd}_6\text{Se}_6\text{L}_9} - E_{\text{Cd}_6\text{Se}_6\text{L}_6} - 3E_L$$

where, ( $\overline{BE}$ ) is the average binding energy for each ligand;  $n$  is the number of ligands in the complex;  $m$  is the number of cadmium and selenium atoms in the quantum dots clusters;  $E_{\text{Cd}_m\text{Se}_m\text{L}_n}$  is the energy of ligand-bound complex;  $E_{\text{Cd}_m\text{Se}_m}$  is the energy of bare cluster;  $E_L$  is the energy of single ligand.  $BE_2$  is the average binding energy for the second ligand molecule on a surface cadmium atom in cluster Cd<sub>6</sub>Se<sub>6</sub>;  $E_{\text{Cd}_6\text{Se}_6\text{L}_6}$  is the energy of complex with six singly capped ligand;  $E_{\text{Cd}_6\text{Se}_6\text{L}_9}$  is the energy of complex including the second ligands on three cadmium atoms.

## Results and Discussions

### Bare Clusters

The optimized geometries of bare cluster and ligand passivated structures of cluster Cd<sub>6</sub>Se<sub>6</sub> and Cd<sub>13</sub>Se<sub>13</sub> are listed in Tables 1 and 2 respectively. The representative

**Table 1** Structural parameters (in Å), HOMO–LUMO gap (in eV), and ligand binding energies (in kcal/mol/ligand) for neutral and doubly charged cluster Cd<sub>6</sub>Se<sub>6</sub> and its complexes capped with ligands

Ligand	Bond lengths (Å)						HOMO–LUMO gap (eV)						Binding energy (kcal/mol/ligand)						
	Cd–Se		Se–Se		Cd–L		B3LYP		OPBE		2+		B3LYP		OPBE		2+		
	B3LYP	OPBE	2+	B3LYP	OPBE	2+	B3LYP	OPBE	2+	B3LYP	OPBE	2+	B3LYP	OPBE	2+	B3LYP	OPBE	2+	
(CdSe) <sub>6</sub>	2.670 <sup>a</sup>	2.686	2.701	4.274	4.264	4.104	–	–	–	–	–	3.14	2.57	0.57	–	–	–	–	–
	2.864 <sup>b</sup>	2.835	2.898																
PH <sub>3</sub>	2.722 <sup>a</sup>	2.711	2.732	4.297	4.293	4.090	2.945	3.016	2.813	3.11	0.62	–9.4	–5.7	–25.3					
	2.862 <sup>b</sup>	2.836	2.860																
2 <sup>nd</sup> PH <sub>3</sub>	2.708 <sup>a</sup>	2.748	2.748	4.301	4.292	4.094	2.974	3.011	2.834	3.11	0.61	–6.4 (–0.36)	–4.2 (–1.1)	–19.0 (–6.4)					
	2.734 <sup>a</sup>	2.711	2.707				3.302	5.810	3.030	2.872									
	2.852 <sup>b</sup>	2.835	2.839																
PMe <sub>3</sub>	2.734 <sup>a</sup>	2.726	2.740	4.314	4.314	4.101	2.851	2.894	2.751	4.11	3.25	0.64	–14.5	–10.3	–35.6				
	2.871 <sup>b</sup>	2.841	2.874																
NH <sub>3</sub>	2.733 <sup>a</sup>	2.726	2.734	4.326	4.321	4.102	2.404	2.434	2.352	3.93	3.14	0.60	–21.9	–17.1	–39.5				
	2.871 <sup>b</sup>	2.846	2.873																
2 <sup>nd</sup> NH <sub>3</sub>	2.711 <sup>a</sup>	2.709	2.710	4.415	4.473	4.297	2.418	2.446	2.377	3.90	3.14	0.59	–17.6 (–9.0)	–12.6 (–3.6)	–32.4 (–182)				
	2.764 <sup>a</sup>	2.778	2.745				2.491	2.470	2.433	2.536									
	2.862 <sup>b</sup>	2.814	2.827																
NMe <sub>3</sub>	2.739 <sup>a</sup>	2.731	2.742	4.325	4.301	4.104	2.427	2.508	2.354	4.14	3.26	0.60	–21.3	–13.2	–39.9				
	2.863 <sup>b</sup>	2.834	2.868																
OPH <sub>3</sub>	2.753 <sup>a</sup>	2.739	2.734	4.304	4.298	4.178	2.273	2.308	2.189	3.67	2.86	0.57	–26.5	–17.5	–47.1				
	2.880 <sup>b</sup>	2.862	2.879																
OPMe <sub>3</sub>	2.750 <sup>a</sup>	2.741	2.745	4.347	4.335	4.253	2.260	2.328	2.168	3.98	3.03	0.58	–28.3	–18.1	–54.9				
	2.887 <sup>b</sup>	2.843	2.874																

The data for charged systems was obtained at B3LYP/LANL2DZ model chemistry (The data in parentheses represent the BE<sub>2</sub> as defined in calculation section.)

<sup>a</sup> Cd–Se bond length within layer

<sup>b</sup> Cd–Se bond length between layers



**Table 2** Structural parameters (in Å), HOMO–LUMO gap (in eV), and ligand binding energies (in kcal/mol/ligand) for neutral and doubly charged Cd<sub>13</sub>Se<sub>13</sub> cluster, passivated by 10 ligands

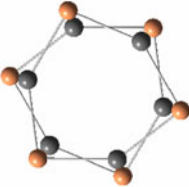
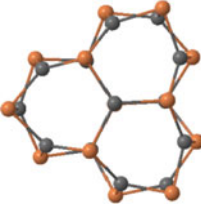
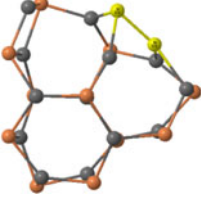
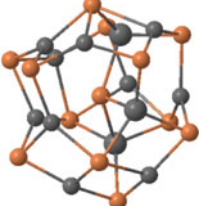
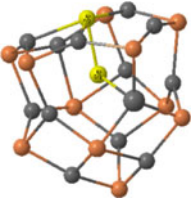
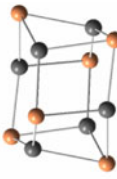
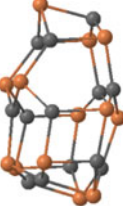
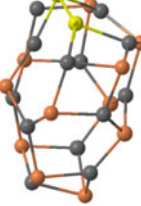
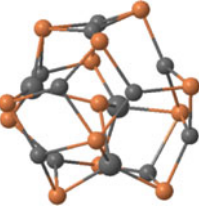
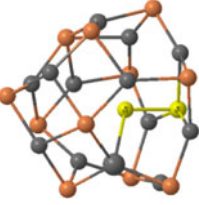
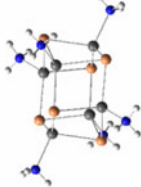
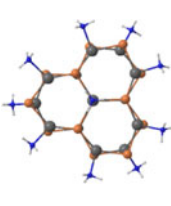
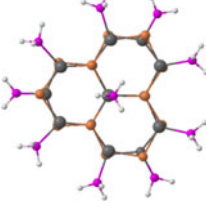
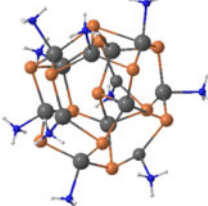
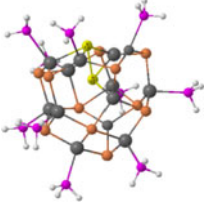
Ligand/charge	Bond lengths (Å)						HOMO–LUMO gap (eV)		Binding energy (kcal/mol/ligand)	
	Cd–Se		Se–Se		Cd–L		Cage	Wurtzite	Cage	Wurtzite
	Cage	Wurtzite	Cage	Wurtzite	Cage	Wurtzite				
Bare/0–	2.766 <sup>a</sup>	2.704 <sup>c</sup>	–	–	–	–	3.18	2.99	–	–
	3.023 <sup>b</sup>	2.785 <sup>d</sup>								
Bare/2+	2.756 <sup>a</sup>	2.660 <sup>c</sup>	2.610	2.655	–	–	2.78	1.70	–	–
	3.164 <sup>b</sup>	2.765 <sup>d</sup>								
PH <sub>3</sub> /0	2.782 <sup>a</sup>	2.722 <sup>c</sup>	–	–	2.995	2.962	3.59	3.50	–7.7	–8.1
	2.876 <sup>b</sup>	2.814 <sup>d</sup>								
PH <sub>3</sub> /2+	2.786 <sup>a</sup>	2.722 <sup>c</sup>	2.615	–	2.906	2.887	2.79	0.38	–15.8	–11.7
	2.982 <sup>b</sup>	2.801 <sup>d</sup>								
PMe <sub>3</sub> /0	2.793 <sup>a</sup>	2.726 <sup>c</sup>	–	–	2.882	2.874	3.71	3.59	–12.4	–12.9
	2.846 <sup>b</sup>	2.819 <sup>d</sup>								
PMe <sub>3</sub> /2+	2.721 <sup>a</sup>	2.732 <sup>c</sup>	2.606	–	2.816	2.789	2.81	0.41	–23.3	–19.4
	2.937 <sup>b</sup>	2.806 <sup>d</sup>				2.892 <sup>e</sup>				
NH <sub>3</sub> /0	2.770 <sup>a</sup>	2.736 <sup>c</sup>	–	–	2.414	2.412	3.52	3.47	–20.2	–20.5
	2.843 <sup>b</sup>	2.823 <sup>d</sup>								
NH <sub>3</sub> /2+	2.716 <sup>a</sup>	2.715 <sup>c</sup>	2.619	–	2.383	2.379	2.71	0.37	–29.1	–25.4
	2.952 <sup>b</sup>	2.821 <sup>d</sup>								
OPH <sub>2</sub> Me/0	2.732 <sup>a</sup>	2.737 <sup>c</sup>	–	–	2.290	2.274	3.42	3.52	–25.8	–27.0
	2.869 <sup>b</sup>	2.845 <sup>d</sup>								
OPH <sub>2</sub> Me/2+	2.710 <sup>a</sup>	2.729 <sup>c</sup>	2.609	–	2.232	2.223	2.80	0.39	–38.2	–34.4
	2.872 <sup>b</sup>	2.838 <sup>d</sup>								

<sup>a</sup> Cd–Se bond length on the cage surface<sup>b</sup> Cd–Se bond lengths between surface Cd and interior Se<sup>c</sup> Cd–Se bond length within a layer in wurtzite structure<sup>d</sup> Cd–Se bond length between layers in wurtzite structure<sup>e</sup> Cd–L bond length in the center of outer layer

– no bond formed between the labeled atoms

geometries are shown in Table 3 from the top and side viewpoints. Surface re-organization and relaxation of the clusters is the main reason for the structure distortion from the ideal wurtzite unit cell, which appears in the crystal bulk structure. In general, cadmium atoms go inside the bulk while selenium atoms tend to go outside during the relaxation process. The optimized structures of Cd<sub>6</sub>Se<sub>6</sub> and Cd<sub>13</sub>Se<sub>13</sub> are in agreement with the recent results reports [111, 115, 118]. For the bare neutral cluster Cd<sub>6</sub>Se<sub>6</sub>, the average Cd–Se bond length in the surface layer is 2.670 and 2.864 Å between layers. Similar observations were found in the Cd<sub>13</sub>Se<sub>13</sub> wurtzite system. The infrastructures of the Cd–Se clusters are predominantly controlled by the cluster surface self-reorganization, which significantly reduces the unsaturated degree of the surface atoms. The cadmium atoms with two dangling

**Table 3** Optimized geometries for bare  $\text{Cd}_{13}\text{Se}_{13}$  and  $\text{Cd}_{13}\text{Se}_{13}^{2+}$  clusters with cage and wurtzite structures

	$(\text{CdSe})_6$ (wurtzite)	$(\text{CdSe})_{13}$ (wurtzite)	$(\text{CdSe})_{13}^{2+}$ (wurtzite)	$(\text{CdSe})_{13}$ (cage)	$(\text{CdSe})_{13}^{2+}$ (cage)
Top view					
Side view					
$\text{NH}_3$ or $\text{PH}_3$					

The Cd, Se, P, C, and H atoms are shown in dark gray, gold, pink, gray, and white respectively. The Se–Se bond formation was highlighted using yellow color in charged clusters

bonds are rearranged to form three coordination bonds and have only one dangling bond left. Our simulations indicate that the surface relaxations behave in a consistent way regardless of the size of quantum dots. This conclusion agrees with previous reports [79, 105].

### *Cage vs. Wurtzite*

It was reported experimentally that there are two types geometry for small magic-size CdSe nanocrystals clusters, wurtzite and cage [127]. The relative stability between these two type structures is an important question for nanocrystals growth. For cluster  $\text{Cd}_6\text{Se}_6$ , these two structures are converged to the same geometry with no atoms inside. But for  $\text{Cd}_{13}\text{Se}_{13}$  cluster, the calculation results show two distinct optimal geometries with cage structure being more stable than the wurtzite one for both bare cluster, as well as ligands passivated complexes, shown in Table 4. For the bare cluster, the cage form has lower energy than the wurtzite structure with difference of 10.40 kcal/mol. As a consequence, wurtzite structure, which is the stable phase for bulk and the core of QDs, is not the most stable morphology for small bare clusters. As shown in the following sections, the relative stability between wurtzite structure and cage structure can be strongly manipulated by surface ligands and surface charges.

### Effects of Ligands

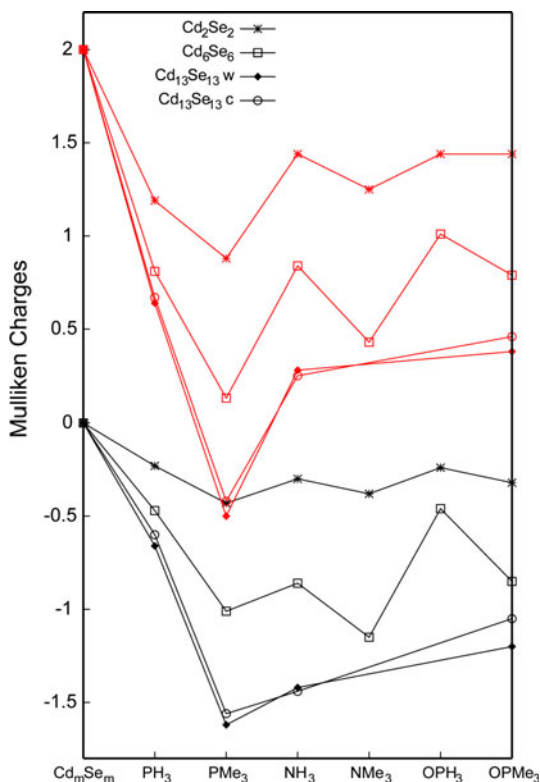
The optimized geometries of CdSe clusters in the complexes capped by ligands are qualitatively same as the relaxed bare clusters, although the Cd–Se bond lengths are slightly lengthened due to the existence of capping ligands donating electronic density to the Cd–Se bond. The cluster self-reorganization is the dominant factor for the surface relaxation. The Cd–Se distances change to 2.734, 2.733, and 2.753 Å for  $\text{PMe}_3$ ,  $\text{NH}_3$ , and  $\text{OPH}_3$  passivated clusters respectively. In general, surface ligands have noticeable effects on the geometry structure, such as the Cd–Se bond lengths on the cluster surface are stretched about 0.1 Å in average. The degree of stretching depends on the type of ligand, degree of passivation, structure of cluster, size of cluster and charges on the complexes.

Capping ligands further remove the dangling bonds on the relaxed surface by donating electrons to the cluster. The Mulliken charge analysis, Fig. 1, shows that the ligands significantly increase the charges on the CdSe clusters (more negative charges) compared to the bare clusters. Not surprisingly, the coordination bond length between Cd atoms and ligands, Cd–L, is highly ligand dependent and in the

**Table 4** Energy difference,  $\Delta E = E_{\text{wurtzite}} - E_{\text{cage}}$ , between wurtzite and cage structures of bare  $\text{Cd}_{13}\text{Se}_{13}$  and passivated  $\text{Cd}_{13}\text{Se}_{13}\text{L}_{10}$  in kcal/mol, calculated at B3LYP/LANL2DZ model chemistry

	$(\text{CdSe})_{13}$	$\text{PH}_3$	$\text{PMe}_3$	$\text{NH}_3$	$\text{OPH}_2\text{Me}$
Charge 0	10.4	6.0	5.8	7.3	−1.4
Charge +2	50.1	40.9	38.7	37.3	37.9

**Fig. 1** The total Mulliken charges on the cluster core in bare and passivated  $Cd_mSe_m$  clusters. The label  $Cd_mSe_m$  represents  $Cd_2Se_2$ ,  $Cd_6Se_6$ , and  $Cd_{13}Se_{13}$  accordingly. The ligands passivating each studied CdSe cluster are shown along the horizontal axis. The 'w' and 'c' in the insert indicate 'wurtzite' and 'cage' structure, respectively. The *black lines* are for the neutral clusters and the *gray/red lines* are for the corresponding doubly cationic clusters. There are no data points for  $NMe_3$  and  $OPH_3$  of the cluster  $Cd_{13}Se_{13}$ . For neutral and cationic clusters  $Cd_{13}Se_{13}$  shown to be ligated with  $OPMe_3$ , the charge values were obtained on systems actually ligated with  $OPH_2Me$  (Color figure online)



order of  $Cd-O < Cd-N < Cd-P$ . The  $Cd-L$  of the neutral  $Cd_6Se_6$  cluster is 2.851 Å for  $PMe_3$ , 2.404 Å for  $NH_3$ , and 2.273 Å for  $OPH_3$ . Those values change to 2.882 Å for  $PMe_3$ , 2.414 Å for  $NMe_3$  and 2.290 Å for  $OPH_2Me$  passivating the neutral  $Cd_{13}Se_{13}$  cluster respectively. Given the Van der Waals radii of phosphorus, nitrogen, and oxygen, (1.80, 1.55 and 1.52 Å respectively), the coordination bond length decreases accordingly in the same order.

### Doubly Passivated Sites

Ideal wurtzite structures exhibit a Cd-rich facet and a Se-rich facet. On the Cd-rich facet, some cadmium atoms are only doubly bounded to their vicinal selenium atoms and need two ligand molecules to be fully passivated. For example, the ideal  $Cd_6Se_6$  wurtzite cluster has three cadmium atoms triply coordinated with their vicinal selenium atoms on the Se-rich facet and three cadmium atoms doubly coordinated on the Cd-rich facet. The triply coordinated cadmium atoms can be capped by single ligand and the doubly coordinated ones initially capped by two ligands. Accordingly, there are 9 ligands required to remove all dangling bonds in the fully passivated  $Cd_6Se_6$ . After geometry relaxation, the core of  $Cd_6Se_6$  reorganized to a cluster with a flatter surface. The cluster structures reorganized in a way that each cadmium atom forms three covalent bonds with neighboring selenium

atoms. The Cd atoms initially having two dangling bonds, become partially saturated by surface reorganization. One of the two ligands tends to dissociate from the cluster as evidenced by the resulting long distance to the cluster. Such as, the distance between cadmium atoms and dissociated  $\text{PH}_3$  ligands is 3.302 Å compared to singly bonded coordination bond length, 2.974 Å.

Though the binding for the second ligand on the same site (Cd atom) is thermodynamically feasible for the chosen ligand models, the average binding energy for the second ligand  $BE_2$  are much smaller than that of for the first ligand, as shown in Table 1 in parentheses. For example,  $BE_2$  for  $\text{NH}_3$  is  $-8.96$  kcal/mol per ligand compared to  $(\overline{BE})$   $-21.89$  kcal/mol. The latter is the average binding energies for the first  $\text{NH}_3$  ligand on cadmium atoms. These values change to  $-0.36$  and  $-9.40$  kcal/mol for  $\text{PH}_3$  ligand, respectively. Given the long and bulky tails in real ligands, coordination of a second ligand on the same site would be more difficult than the first one because of increased steric interactions. Furthermore, facets will be formed when the sizes of quantum dots get larger resulting in more surface atoms on the facets with less-curvature than on the edges. As a result, the possibility is rare to have double passivation on one atomic site. From now on, the double passivation for one Cd atom is not further considered in the following calculations.

We observed that ligands do not bind to Se atom in the minimal cluster,  $\text{Cd}_2\text{Se}_2$ , in our previous work [104]. The calculations for larger clusters,  $\text{Cd}_6\text{Se}_6$  and  $\text{Cd}_{13}\text{Se}_{13}$ , show that there is no thermodynamically favorable binding on Se atom regardless the size of cluster and the type of ligands. Our observation is different from the report that stated amine was observed to bind stronger with Se atoms than Cd atoms [79]. Unless otherwise specified, we will focus on discussing single passivation Cd atoms and no passivation on Se atoms for the chosen clusters and ligand models.

### Ligand Electronegativity

The simplest model for trimethylphosphine (TOP),  $\text{PH}_3$ , produced essentially same core geometries compared to its most complicated and realistic sibling model,  $\text{PMe}_3$ . The variations of Cd–Se bonds are within 0.06 Å. The addition of extra three methyl groups brings the ligands closer to cadmium atoms by 0.1 Å by providing more electron donation. The same observation is found for all the cluster sizes studied including  $\text{Cd}_2\text{Se}_2$ ,  $\text{Cd}_6\text{Se}_6$ , and  $\text{Cd}_{13}\text{Se}_{13}$ .  $\text{PH}_3$  is an excellent simple model to study the geometries of quantum dots passivated by TOP. However, when the binding energies are taken into account, the substitution of methyl group for hydrogen atoms in  $\text{PH}_3$  is important. The average binding energy for  $\text{PMe}_3$  is  $-14.45$  kcal/mol increased from  $-9.40$  kcal/mol for  $\text{PH}_3$  for the cluster  $\text{Cd}_6\text{Se}_6$ . The average binding energies for ligands  $\text{PH}_2\text{Me}$  and  $\text{PHMe}_2$  stay in between,  $-11.36$  kcal/mol and  $-13.32$  kcal/mol, respectively. The addition of methyl group increases the electronegativity of coordination atom phosphor resulting in the incremental of binding energy. Charge analysis shows that  $\text{PMe}_3$  is a stronger electron donor than  $\text{PH}_3$ , Fig. 1. This observation is found for the larger cluster

$\text{Cd}_{13}\text{Se}_{13}$  as well. Overall, binding energy increases by 50–60% when going from  $\text{PH}_3$  to  $\text{PMe}_3$ . For cluster  $\text{Cd}_{13}\text{Se}_{13}$ , the binding energies are  $-12.46$ ,  $-15.14$ ,  $-17.30$  and  $-19.18$  kcal/mol for  $\text{PH}_3$ ,  $\text{PH}_2\text{Me}$ ,  $\text{PHMe}_2$ , and  $\text{PMe}_3$ , correspondingly. Thus, the fully methyl substituted Phosphine, i.e.  $\text{PMe}_3$  is needed as ligand model in order to evaluate the binding energy for surface ligand TOP.

In contrast to phosphine, substitution of methyl groups of hydrogen atoms on amine has less impact on both geometries and binding energies, which is less than 2% compared to those for  $\text{NH}_3$ . Trimethylamine has the binding energy almost identical to that of  $\text{NH}_3$ . As a result, amines could be adequately modeled by  $\text{NH}_3$  in the accuracy of geometry parameters and binding energies. The binding energies are at the order of  $-20$  kcal/mol and is in great agreement with experimental measurement of  $-25$  kJ/mol for short-chain amine on CdSe [65].

The trimethylphosphine oxide (TOPO) is the most widely used ligand in syntheses of CdSe quantum dots. The effects of substitution of methyl group on the models of TOPO, from  $\text{OPH}_3$  to  $\text{OPMe}_3$ , are negligible on the geometries of the CdSe clusters. Our observation is consistent with the work reported by Galli's group [79]. In terms of binding energies, the effects are only slightly larger than amine, which decrease when the cluster size increases. For example, the binding energies for  $\text{Cd}_6\text{Se}_6$  change from  $-26.47$  to  $-28.30$  kcal/mol (6.9% increase) from  $\text{OPH}_3$  to  $\text{OPMe}_3$ . These observations suggest that it is sufficient to use  $\text{OPH}_3$  as computational model for TOPO for small CdSe clusters. Nevertheless, we notice for larger  $\text{Cd}_{13}\text{Se}_{13}$  cluster, because of closer distance between ligands on the same facet, very strong hydrogen bonding interactions are formed between ligands, which can cause proton transfer phenomena between ligands and result in unphysical structures being different from synthetically attainable morphologies. Although the fully methylated  $\text{OPMe}_3$  structure provides accurate simulation of TOPO capping agent, it gets too expensive for large clusters with large number of capping ligands. Our calculations show that one addition of methyl group to the phosphine oxide could effectively prevent the proton transfer between ligands and give good results for both geometries and binding energies. Therefore,  $\text{OPH}_2\text{Me}$  is a more appropriate model candidate than  $\text{OPH}_3$  to simulate TOPO capping on quantum dots.

### Size Dependency

The optimized wurtzite structures of  $\text{Cd}_6\text{Se}_6$  and  $\text{Cd}_{13}\text{Se}_{13}$  capped by  $\text{PH}_3$  are alike, the Cd–Se bond length within layer is  $2.732$  Å for  $(\text{Cd}_6\text{Se}_6)(\text{PH}_3)_6$  and  $2.722$  Å for  $(\text{Cd}_{13}\text{Se}_{13})(\text{PH}_3)_{10}$ , which is a sign of that the relaxed surface structure might be similar for clusters with different sizes. The binding pattern for each ligand is kept intact when the cluster size increased. For example, the coordinating bond lengths between Cd–P are  $2.811$ ,  $2.851$  and  $2.882$  Å for cluster  $\text{Cd}_2\text{Se}_2$ ,  $\text{Cd}_6\text{Se}_6$ , and  $\text{Cd}_{13}\text{Se}_{13}$  passivated by  $\text{PMe}_3$ , correspondingly. Similar trend was observed for ligand  $\text{NH}_3$ , the Cd–N bond lengths are  $2.401$ ,  $2.404$  and  $2.414$  Å, respectively. The geometry changes subtly as the cluster size increases, as a result, the ligand binding information collected from these small clusters could be extrapolated to large clusters. It is noteworthy that larger structures foster steric interactions among ligands because the average binding energy for each ligand reduces from  $-12.46$  to

−9.40 to −7.71 kcal/mol with increasing the size of the cluster, which is consistent with recent work by Nguyen et al. [118].

### *Cage vs. Wurtzite*

The optimized geometries of  $\text{Cd}_{13}\text{Se}_{13}$  in cage form and wurtzite structure for ligands passivated complexes are shown in Table 4. Wurtzite structure of bare cluster  $\text{Cd}_{13}\text{Se}_{13}$  is less stable than the cage form by giving energy rise of 10.40 kcal/mol. The ligands stabilize the wurtzite structure slightly more than the cage structure for neutral  $\text{Cd}_{13}\text{Se}_{13}$  cluster by about 0.5–1.0 kcal/mol in terms of the average binding energy per ligand, as listed in Table 2. Therefore, the accumulative energy difference between cage and wurtzite structure for passivated complexes decreases to 6.02, 5.83 and 7.27 kcal/mol, respectively, for  $\text{PH}_3$ ,  $\text{PMe}_3$  and  $\text{NH}_3$  ligand agents. The only ligand stands out is  $\text{OPH}_2\text{Me}$ , which reverses the relative stability order and causes the wurtzite structure to be slightly more stable than the cage form by 1.39 kcal/mol. This is the only wurtzite complex observed to be more stable than the cage complex.

The positive two charges on the clusters bring the cage structure to be more stable by about 37–50 kcal/mol, as shown in Table 4, because all ligands bind to the cage structure by about 4 kcal/mol stronger than to the wurtzite form. These data imply that the cage structure can stably exist at the early stage of the colloidal quantum dots synthesis.

### *Binding Energies*

The binding energy listed in Tables 1 and 2 are averaged binding energies for each ligand molecule. Closely correlated to coordination bond lengths, the binding energies are anticipated to be in the order: phosphine oxide, amines, amine, and phosphine, i.e.  $\text{Cd-O} > \text{Cd-N} > \text{Cd-P}$ . The average binding energy of each ligand is roughly at the order of −25 kcal/mol for phosphine oxide, −20 kcal/mol for amines and −10 kcal/mol for phosphines. The relative binding strength of these ligands is consistent regardless the size of clusters and the charges on the clusters, as shown in Tables 1 and 2. Therefore, this relative binding strength order can be extrapolated to large quantum dots as synthesized experimentally, and can be used to guide the ligand exchange process.

By increasing the cluster size, the average binding energy per ligand becomes smaller for each type of ligands. For example, binding energies for one  $\text{PMe}_3$  to  $\text{Cd}_2\text{Se}_2$ ,  $\text{Cd}_6\text{Se}_6$ , and  $\text{Cd}_{13}\text{Se}_{13}$  clusters are −19.18, −14.45 and −12.40 kcal/mol, correspondingly. With the increase of ligands number on same dots, the steric interactions between ligands increase and the interaction energies between ligands and cluster decrease accordingly. The binding energy for each ligand type will converge to a constant number when cluster size is large. These interactions could be shed light on by calculating step-wise binding energy. The difference between the step-wised binding energies and the average binding energy was tested for

cluster  $\text{Cd}_6\text{Se}_6$  using the equations described here. Because these energies are specifically defined for one cluster, we list them in this session instead of in the session for the general computational details. We define:

$$\begin{aligned}\overline{{}_6BE} &= \frac{1}{6}(E_{\text{Cd}_6\text{Se}_6L_6} - E_{\text{Cd}_6\text{Se}_6} - 6E_L) \\ {}_6BE_1 &= E_{\text{Cd}_6\text{Se}_6L} - E_{\text{Cd}_6\text{Se}_6} - E_L \\ {}_6BE_n &= E_{\text{Cd}_6\text{Se}_6L_6} - E_{\text{Cd}_6\text{Se}_6L_5} - E_L \\ {}_6BE_{1,n} &= \frac{1}{2}({}_6BE_1 + {}_6BE_n)\end{aligned}$$

where,  $\overline{{}_6BE}$  is the average binding energy for all ligands in cluster  $\text{Cd}_6\text{Se}_6$ ;  $E_{\text{Cd}_6\text{Se}_6L_6}$  is the energy of ligand-bound complex;  $E_{\text{Cd}_6\text{Se}_6}$  is the energy of bare cluster;  $E_L$  is the energy of single ligand.  ${}_6BE_1$  is the binding energy for the first ligand molecule on cluster  $\text{Cd}_6\text{Se}_6$ ;  $E_{\text{Cd}_6\text{Se}_6L}$  is the energy of the complex with one ligand;  $E_{\text{Cd}_6\text{Se}_6L_5}$  is the energy of complex with five ligands.  ${}_6BE_n$  is the binding energy for the last ligand molecule to form a fully passivated structure.  ${}_6BE_{1,n}$  is the average binding energy between the first ligand and the last ligand.

The results show that  $\overline{{}_6BE}$  equals to  ${}_6BE_{1,n}$  for every type of ligands within an error tolerance of 0.2 kcal/mol. The binding energy gradually decreases from the first ligand to the last one, i.e.  ${}_6BE_1 > {}_6BE_n$ , because the last ligand encounters the most steric interactions from other bound ligands. The variation between  ${}_6BE_1$  and  ${}_6BE_n$  from the average binding energy ( $\overline{{}_6BE}$ ) is within 4.9 kcal/mol. As a consequence, the difference between the binding energies for the first ligand molecule and the last one can be up to 10 kcal/mol. Although the last ligand molecule binds to the cluster with the smallest binding energy, the binding is still a thermodynamically favorable. For example, for a ligand  $\text{PMe}_3$ ,  ${}_6BE_1$  is  $-19.35$  kcal/mol and  ${}_6BE_n$  is  $-9.89$  kcal/mol, whereas these numbers become  $-25.64$  and  $-18.61$  kcal/mol for a ligand  $\text{NH}_3$ . The competition between the binding interactions from dots and the steric interactions from ligands will reach an equilibrium point in large quantum dots.

### Charge Effects

In synthesis of colloidal quantum dots,  $\text{Cd}^{2+}$  ions are used in solution and could possibly cause the quantum dots to carry the net positive charges. The charged dots have different electronic properties compared to the neutral ones. The complexes carrying two positive charges have been re-optimized to investigate the charge effects on the geometric structures and electronic properties. Previous reported work focused on studying neutral clusters interacting with negatively charged ligands, while we will discuss the effects from positive charges carried by the  $\text{CdSe}$  clusters.

Overall, the positively charged clusters have essentially the same geometries compared to the neutral clusters with only marginal bond length changes for the  $\text{Cd}_6\text{Se}_6$  based structures. The charges on the cluster slightly stretch the  $\text{Cd-Se}$  bond lengths both within and between the layers due to the charge distribution on the surfaces, for both bare and passivated clusters. The  $\text{Cd}_6\text{Se}_6^{2+}$  cluster shows the



tendency to form a Se–Se bond as evidenced by shrinkage of Se–Se bond by about 0.20–0.25 Å. However, due to the geometric constraints of wurtzite structure, formation of a Se–Se bond is prohibited. The charges cause flatter layers by reducing the dihedral angles within a layer from  $\sim 26^\circ$  to  $\sim 6^\circ$ . The positive charges on the cluster cause the coordination bond lengths (Cd–L) shortened by 0.07–0.13 Å. Phosphine ligands have the largest change, then phosphine oxide, and finally, amine changes the least as shown in Table 4. This is consistent with the polarizability of the coordinating atoms. Due to deficiency of charges on Cd atoms, the ligands are brought closer to the cluster to sharing more electron density to the cluster and enhance the interactions with ligands. As shown in Fig. 1, the charge analysis shows that ligands on charged dots donate more electrons to the CdSe cluster. For example, the charges on the neutral cluster change from 0 to  $-1.01$  after passivated by  $\text{PMe}_3$ ; whereas the charges on the positively charged cluster changes from  $+2.0$  to  $+0.13$  after passivated by the same ligand. As a consequence, the binding energies increase by approximately 150% for phosphine and 80% for amines and trisphosphine oxide.

In the case of wurtzite structure of bare  $\text{Cd}_{13}\text{Se}_{13}$  clusters, the deficiency of charge on the cluster causes the surface reorganization forming a Se–Se bond, shown in Table 3. The coordination distances between ligands and Cd atoms (Cd–L) in passivated complexes to shorten from 0.03 to 0.09 Å. This change of the Cd–L bond length is smaller than that of the  $\text{Cd}_6\text{Se}_6$  cluster, because of the charges distribution over the larger cluster. As a result, the increase of binding energies is smaller compared to the  $\text{Cd}_6\text{Se}_6$  cluster. For the cage structure of  $\text{Cd}_{13}\text{Se}_{13}$  clusters, the charged species result higher binding energies by approximately 100% for phosphine and 50% for amine and trisphosphine oxide. These values reduce to half for the wurtzite structures, i.e. 50% for phosphine and 25% for amine and trisphosphine oxide.

### *Se–Se Bond Formation*

Charges on the  $\text{Cd}_{13}\text{Se}_{13}$  clusters cause more geometric change to the cage structure than to the wurtzite structure. In the cage form, the positive charges ( $+2$ ) on the surfaces cause the formation of Se–Se bond between the central selenium atom and a surface selenium atom at a bond length of 2.6 Å. Subsequently, the central Se atom breaks the bonding with the three surface Cd atoms in neutral form resulting the shortest distance to Cd atoms as 3.2 Å, shown in Table 3. This Se–Se covalent bond formation stabilizes the systems and results in much higher chemical energy difference from the wurtzite structure for both bare and passivated clusters. For the wurtzite form, only the bare cluster has a Se–Se bond formed between layers which cause a fairly large distortion from the original six-ring geometry. The charged wurtzite structure of  $\text{Cd}_{13}\text{Se}_{13}$  only shows the tendency to form Se–Se bond with a reduced Se–Se distance but no actual Se–Se bond is formed. This owes to the effective charge re-distributions on the ligands, compared to the bare wurtzite cluster whose charges are distributed on the cluster only.

### Bridged Bonding Pattern

In fact, due to the bulky volume of ligands, even completely singly passivated pattern may not be achieved due to steric interactions among ligands. There is a possibility that one ligand coordinates to more than one surface atoms to partially saturate dangling bonds. We test this feasibility in this work. One selenium atom in the  $\text{Cd}_6\text{Se}_6$  cluster was removed and substituted by a ligand resulting in a ligand binding to two Cd atoms initially. The complexes ( $\text{Cd}_6\text{Se}_5\text{L}$ ) carry either zero or positive charges (+2), where L is  $\text{PH}_3$ ,  $\text{PMe}_3$ ,  $\text{NH}_3$  and  $\text{OPH}_3$ . A metal Cd–Cd bond (2.91–2.92 Å) forms in the neutral complexes, and the ligand moves away from the center of the two initially bound Cd atoms and become singly coordinated to one Cd atom. When these complexes carry two positive charges, the two Cd atoms repel each other apart 5–6 Å away and resulting the ligand singly bound to one Cd atoms. These results indicate that ligands  $\text{PH}_3$ ,  $\text{PMe}_3$ , and  $\text{NH}_3$  cannot form a bridging coordination bond between two surface cadmium atoms both in neutral and positively charged clusters. In contrast, the ligand  $\text{OPH}_3$  stands out. In the neutral complex,  $\text{OPH}_3$  is chemically dissociated to  $\text{PH}_3$  and an oxygen atom. The generated  $\text{PH}_3$  acts as a capping ligand to a cadmium atom. The oxygen atom takes the position of the removed Se atom and is shared between two surface Cd atoms by forming covalent Cd–O bonds with distances 2.125 Å. In the positively charged complex, the  $\text{OPH}_3$  is kept in its original chemical form and shared by two Cd atoms. The Cd–O distances are 2.409 Å. From these observations, in theory we anticipate that trisphosphine oxide can form bridging coordination bonds on surfaces of a charged CdSe cluster. Delicate experimental measurements would be critical to verify this conclusion in the future.

From the orbital analysis shown in Table 5, the majority of HOMO densities of bare neutral  $\text{Cd}_{13}\text{Se}_{13}$  including both cage and wurtzite structures are localized on surface Se atoms, while the LUMOs locate on the surface Cd atoms. Since interactions between ligands and quantum dots can be considered at donor–acceptor interactions, Cd atoms are able to accept electrons from the lone pairs of ligands to their LUMOs. The charge induced density re-organization changes the localization of frontier orbitals, such as the LUMO of  $\text{Cd}_{13}\text{Se}_{13}^{2+}$  located at the Se–Se bond, which is delocalized on surface Cd atoms in the neutral systems. It is worthy to point out that the HOMO and LUMO of the charged and capped wurtzite structures ( $\text{Cd}_{13}\text{Se}_{13}(\text{OPH}_2\text{Me})_{10}^{2+}$ ), are essentially same as in the bare neutral cluster ( $\text{Cd}_{13}\text{Se}_{13}^0$ ) but with a smaller amplitude. This is because the charges on the core structure are effectively re-distributed on the capping ligands and leaving the electronic states of the core roughly identical to the bare neutral cluster. Furthermore, we tested this idea on a larger cluster  $\text{Cd}_{19}\text{Se}_{20}$ , as a neutral complex formed by a  $\text{Cd}_{19}\text{Se}_{19}^{2+}$  and a  $\text{Se}^{2-}$  ion, shows the similar behavior of surface reorganization by forming Se–Se covalent bond on the Se-rich facet. These charge effects are very important for the optical properties of quantum dots. The capping ligands cannot completely compensate the optical properties destroyed by extra charges, due to the surface reorganization and the formation of Se–Se bond.

**Table 5** HOMO and LUMO of bare and ligated  $Cd_{13}Se_{13}$  and  $Cd_{13}Se_{13}^{2+}$  with cage and wurtzite structures

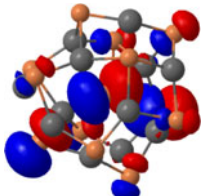
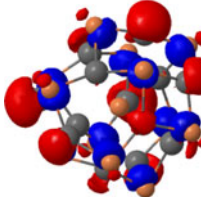
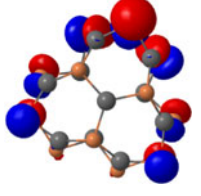
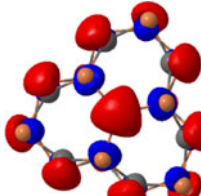
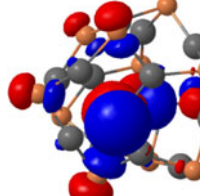
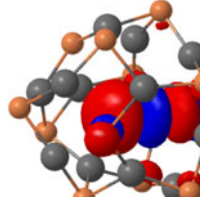
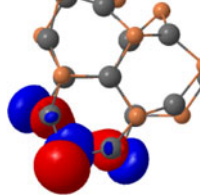
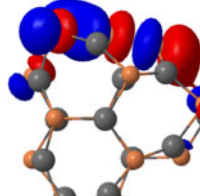
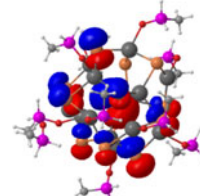
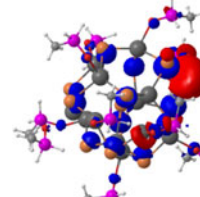
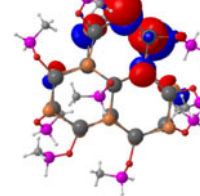
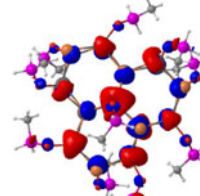
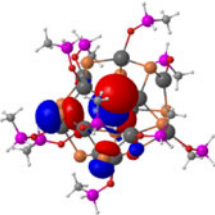
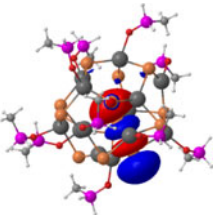
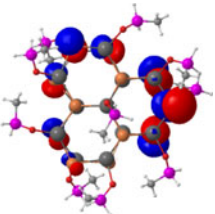
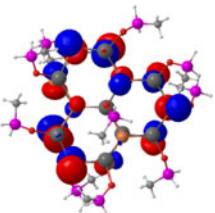
	Cage		Wurtzite	
	HOMO	LUMO	HOMO	LUMO
$(CdSe)_{13}$				
$(CdSe)_{13}^{2+}$				
$(CdSe)_{13}L_{10}$				

Table 5 continued

	Cage		Wurtzite	
	HOMO	LUMO	HOMO	LUMO
(CdSe) <sub>13</sub> L <sub>10</sub> <sup>2+</sup>				

The ligand L is OPH<sub>2</sub>Me. The Cd, Se, P, O, C, and H atoms are shown in dark gray, gold, pink, red, gray, and white colors, respectively

## Optical Properties

Time-dependent Density Functional (TD-DFT) calculations were carried out for selected  $\text{Cd}_{13}\text{Se}_{13}$  clusters. The lowest five singlet excitation energies for both cage and wurtzite structure of cluster  $\text{Cd}_{13}\text{Se}_{13}$ , including the capped complexes and charged species, are listed in Table 6. The lowest two excitations are degenerate for most structures. Comparing those data with HOMO–LUMO gaps in Table 2, the HOMO–LUMO gaps for neutral systems are consistently larger than first excitation energies for the same systems by about 0.5 eV. This suggests that the single-particle orbital energies can serve a reasonable zero-order approximation to the main optical transitions. Indeed Coulombic correlation effects in quantum dots have been considered in a perturbation approach in majority of previous modeling. Capping ligands further amplify the energy gap for semiconductor quantum dots. When the cage structure of cluster  $\text{Cd}_{13}\text{Se}_{13}$  is passivated by ligands  $\text{NH}_3$ , the lowest excitation energy, singlet, becomes 2.988 eV from 2.665 eV. For the wurtzite structure, the lowest excitation is also singlet and the energy shifts up to 2.979 eV from 2.503 eV after passivated by  $\text{NH}_3$ . These values are approximately equal to the respective shifts of HOMO–LUMO gaps. These observations indicate that Kohn–Sham transitions can be used to identify trends in the optical gap behavior for large quantum dots when TDDFT calculations are not computationally affordable.

As shown in the structural effects and energetics of ligand binding, charges also have profound effects on the optical properties on quantum dots. When two electrons are removed, the highest occupied molecular orbital in neutral species becomes a virtual orbital in charged clusters. Because its orbital energy is very close to its next lower molecular orbital (HOMO-1), this new virtual orbital becomes a mid-gap state if no self-reorganization occurs. For example, in the  $\text{Cd}_6\text{Se}_6$  cluster, the charged species have essentially the same structures as their neutral counterparts, the HOMO–LUMO gaps are around 0.6 eV. This is also observed in the ligand capped wurtzite structures of  $\text{Cd}_{13}\text{Se}_{13}$ , which give the gaps around 0.4 eV. It is not surprising that surface relaxation changes the story. The charged cage structures of  $\text{Cd}_{13}\text{Se}_{13}$ , regardless the existence of ligands, give energy gaps around 2.8 eV. The mid-gap state is effectively removed by forming a Se–Se covalent bond. This conclusion can also be verified by exploring the energy gap, 1.70 eV, given by relaxed bare wurtzite structure of  $\text{Cd}_{13}\text{Se}_{13}^{2+}$  with a Se–Se bond at 2.655 Å. This gap is much larger than the corresponding ligand capped wurtzite complexes (lower than 0.4 eV) because the ligands effectively redistribute the charges and prevent the formation of Se–Se bond. TD-DFT results shown in Table 6 also confirm the conclusions derived from the energy gap analysis. It is noteworthy that the excitation energies for the charged cage species are smaller than their neutral counterparts after including the geometric relaxation. These excitation energies can be affected slightly by the type of ligands, such as, the first excitation energies for  $(\text{CdSe})_{13}(\text{NH}_3)_{10}^{2+}$  and  $(\text{CdSe})_{13}(\text{PH}_3)_{10}^{2+}$  in their cage structure are 2.06 and 2.15 eV, respectively.

Surface self-reorganization is the predominate factor to remove the mid-states and opening up the band gap for quantum dots. Calculated HOMO–LUMO gaps of studied clusters are listed in Tables 1 and 2. The HOMO–LUMO gap for relaxed

**Table 6** Excitation energies  $E$  (eV) and oscillator strength, Osc. (unitless) of the lowest five singlet excited states for clusters of  $\text{Cd}_{13}\text{Se}_{13}$  and  $\text{Cd}_{13}\text{Se}_{13}^{2+}$  in cage and wurtzite structure

	1st state	2nd state	3rd state	4th state	5th state
<i>Cage</i>					
$(\text{CdSe})_{13}$					
$E$ (eV)	2.67	2.67	2.76	2.86	3.09
Osc.	0.050	0.050	0.058	0.008	0.021
$(\text{CdSe})_{13}(\text{NH}_3)_{10}$					
$E$ (eV)	2.99	3.06	3.06	3.33	3.39
Osc.	0.082	0.109	0.109	0.015	0.081
$(\text{CdSe})_{13}(\text{PH}_3)_{10}$					
$E$ (eV)	3.10	3.10	3.11	3.44	3.44
Osc.	0.100	0.101	0.093	0.018	0.018
$(\text{CdSe})_{13}^{2+}$					
$E$ (eV)	2.12	2.26	2.41	2.43	2.55
Osc.	0.010	0.003	0.007	0.001	0.003
$(\text{CdSe})_{13}(\text{NH}_3)_{10}^{2+}$					
$E$ (eV)	2.06	2.16	2.25	2.33	2.44
Osc.	0.006	0.002	0.002	0.001	0.003
$(\text{CdSe})_{13}(\text{PH}_3)_{10}^{2+}$					
$E$ (eV)	2.15	2.21	2.39	2.41	2.54
Osc.	0.005	0.004	0.002	0.002	0.002
<i>Wurtzite</i>					
$(\text{CdSe})_{13}$					
$E$ (eV)	2.50	2.50	2.63	2.79	2.79
Osc.	0.009	0.009	0.027	0.015	0.015
$(\text{CdSe})_{13}(\text{NH}_3)_{10}$					
$E$ (eV)	2.98	2.98	3.10	3.12	3.19
Osc.	0.013	0.014	0.079	0.012	0.027
$(\text{CdSe})_{13}(\text{PH}_3)_{10}$					
$E$ (eV)	3.01	3.01	3.10	3.17	3.17
Osc.	0.013	0.013	0.089	0.011	0.011
$(\text{CdSe})_{13}^{2+}$					
$E$ (eV)	1.38	1.64	1.75	1.77	1.81
Osc.	0.0006	0.0007	0.001	0.005	0.001
$(\text{CdSe})_{13}(\text{NH}_3)_{10}^{2+}$					
$E$ (eV)	0.19	0.26	0.33	0.34	0.38
Osc.	0.006	0.004	0.007	0.001	0.011
$(\text{CdSe})_{13}(\text{PH}_3)_{10}^{2+}$					
$E$ (eV)	0.11	0.18	0.32	0.34	0.36
Osc.	0.002	0.002	0.010	0.002	0.009

bare wurtzite structure of  $\text{Cd}_6\text{Se}_6$  is 3.14 eV while the single point calculation for the ideal wurtzite structure of  $\text{Cd}_6\text{Se}_6$  gives the HOMO–LUMO gap 0.67 eV. Similarly, for  $\text{NH}_3$  capped structure, the HOMO–LUMO gap is 3.93 eV while single point calculation predicts the HOMO–LUMO gap for the capped ideal wurtzite structure having 0.88 eV. Another example is the HOMO–LUMO gap for the charged  $\text{Cd}_{13}\text{Se}_{13}^{2+}$  at optimized neutral geometry being 0.34 eV, while the relaxed charged species have gives 1.70 eV gap with a new Se–Se bond.

Meanwhile, the capping of ligands further stabilizes the cluster and broadens the band gap. For example, the HOMO–LUMO gap for the optimized cage structure of  $\text{Cd}_{13}\text{Se}_{13}$  is 3.18 eV, and those for complexes capped by phosphine, amine and phosphine oxide are slightly higher with gaps as 3.59, 3.52 and 3.42 eV respectively. This observation is common for all the structures discussed in this work. The difference between HOMO–LUMO gaps of capped complexes and bare cluster for  $\text{Cd}_6\text{Se}_6$  is larger than that for  $\text{Cd}_{13}\text{Se}_{13}$ , as shown in Table 1 and 2. With the increase of cluster size, the ratio of the surface atoms in the clusters reduces; as a result the ligand impact decreases. Overall, our calculations show that the optical properties are predominately controlled by the core structure with inclusion of surface reorganization. Furthermore, these optical properties can be finely tuned by surface ligands.

## Summary

The chemistry between CdSe quantum dots and common surface capping ligands has been investigated using DFT. We discuss the electronic structures and optical properties of CdSe QDs controlled by the size of particle, self-organization, capping ligands, and positive charges. The chosen model ligands reproduce good structural and energetic description of the interactions between the ligands and quantum dots. In order to capture the proper chemical nature and energetics of the interactions between the capping ligands and CdSe quantum dots, we found that  $\text{PMe}_3$  is needed to adequately simulate TOP and  $\text{NH}_3$  is sufficient for amines.  $\text{OPH}_2\text{Me}$  should be used to simulate TOPO. There is no energetically favorable binding of ligands on Se atom regardless the size of cluster and the type of ligands. Ligands phosphine and amines cannot form a bridging coordination bond between two surface cadmium atoms, while TOPO could form bridging bonds on a surface charged CdSe cluster. Our calculations show that the core structures of CdSe clusters are predominantly controlled by the cluster self-organization and insensitive to the type of surface ligands. The relative binding interaction strength between ligands is in order:  $\text{Cd–O} > \text{Cd–N} > \text{Cd–P}$ . The averaged binding energy per ligand is roughly at the order of  $-25$  kcal/mol for TOPO,  $-20$  kcal/mol for amines and  $-10$  kcal/mol for phosphine. This relative order shows little dependence on the size of clusters or the charges on the clusters and thus may be extrapolated to large quantum dots.

Charges on quantum dots have profound effects on the structures, binding energies, and optical properties. For small cluster  $\text{Cd}_6\text{Se}_6$ , charges have small effects on the structure reorganization but large effects on the energy gaps. The mid-state formed by introducing charges can be effectively removed by forming a Se–Se

bond in the cage structures of  $\text{Cd}_{13}\text{Se}_{13}$  and the bare wurtzite structure. Our calculations show that in general the optical properties are predominately controlled by the core structure with inclusion of surface reorganization. Furthermore, these optical properties can be finely tuned by surface ligands. In this work, TDDFT analysis clues that HOMO–LUMO gap can be used for optical properties analysis for large quantum dots when time-dependent excitation calculations are not feasible. These studies will provide the motivation for future exploration of the capping effects in this fascinating class of quantum dots. The work described above represents the steps toward establishing a knowledge pool of quantum dots by characterizing their chemical and electronic properties at the interface between QDs and surface ligands, and eventually to enable scientists to catalog a desired set of properties of quantum dots for an application, and to design and synthesize the QDs to meet these specific requirements in a controlled way, to create QDs with controlled dimensionality and tunable electronic properties.

**Acknowledgments** PY acknowledges support from Environmental Molecular Sciences Laboratory (a national scientific user facility sponsored by the U.S. Department of Energy's Office of Biological and Environmental Research) located at Pacific North-west National Laboratory and operated for the DOE by Battelle. ST acknowledges support of the Center for Advanced Solar Photophysics (CASAP), an Energy Frontier Research Center funded by the U.S. Department of Energy (DOE). We acknowledge support of Center for Integrated Nanotechnology (CINT) and Center for Nonlinear Studies (CNLS). Los Alamos National Laboratory is operated by Los Alamos National Security, LLC, for the National Nuclear Security Administration of the U.S. Department of Energy under contract DE-AC52-06NA25396.

## References

1. C. B. Murray, D. J. Norris, and M. G. Bawendi (1993). *J. Am. Chem. Soc.* **115**, 8706.
2. X. G. Peng, L. Manna, W. D. Yang, J. Wickham, E. Scher, A. Kadavanich, and A. P. Alivisatos (2000). *Nature* **404**(6773), 59.
3. L. Manna, D. J. Milliron, A. Meisel, E. C. Scher, and A. P. Alivisatos (2003). *Nat. Mater.* **2**, 382.
4. P. V. Kamat (2008). *J. Phys. Chem. C* **112**, 18737.
5. P. V. Kamat (2007). *J. Phys. Chem. C* **111**, 2834.
6. J. Y. Lek, L. F. Xi, B. E. Kardynal, L. H. Wong, and Y. M. Lam (2011). *ACS Appl. Mater. Interfaces* **3**, 287.
7. I. Lokteva, N. Radychev, F. Witt, H. Borchert, J. Parisi, and J. Kolny-Olesiak (2010). *J. Phys. Chem. C* **114**, 12784.
8. M. Bruchez Jr, M. Moronne, P. Gin, S. Weiss, and A. P. Alivisatos (1998). *Science* **281**, 2013.
9. D. Gerion, F. Pinaud, S. C. Williams, W. J. Parak, D. Zanchet, S. Weiss, and A. P. Alivisatos (2001). *J. Phys. Chem. B* **105**, (37), 8861.
10. N. Tessler, V. Medvedev, M. Kazes, S. Kan, and U. Banin (2002). *Science* **295**, 1506.
11. J. M. Caruge, J. E. Halpert, V. Wood, V. Bulovic, and M. G. Bawendi (2008). *Photonics* **2**, 247.
12. L. Bakueva, S. Musikhin, M. A. Hines, T.-W. F. Chang, M. Tzolov, G. D. Scholes, and E. H. Sargent (2003). *Appl. Phys. Lett.* **82**, 2895.
13. D. A. Tryk, A. Fujishima, and K. Honda (2000). *Electrochim. Acta* **45**, 2363.
14. W. J. Parak, D. Gerion, T. Pellegrino, D. Zanchet, C. Micheel, S. C. Williams, R. Boudreau, M. A. Le Gros, C. A. Larabell, and A. P. Alivisatos (2003). *Nanotechnology* **14**, (7), R15.
15. X. Michalet, F. Pinaud, T. D. Lacoste, M. Dahan, M. P. Bruchez, A. P. Alivisatos, and S. Weiss (2001). *Single Mol.* **2**, (4), 261.
16. X. Michalet, F. Pinaud, L. A. Bentolila, J. M. Tsay, S. Doose, J. J. Li, G. Sundaresan, A. M. Wu, S. S. Gambhir, and S. Weiss (2005). *Science* **307**, 538.
17. I. L. Medintz, H. T. Uyeda, E. R. Goldman, and H. Mattoussi (2005). *Nat. Mater.* **4**, 435.
18. R. Gill, M. Zayats, and I. Willner (2008). *Angew. Chem. Int. Ed.* **47**, 7602.



19. A. B. Ellis, R. J. Brainard, K. D. Kepler, D. E. Moore, E. J. Winder, and T. F. Kuech (1997). *J. Chem. Educ.* **74**, 680.
20. M. Nirmal, B. O. Dabbousi, M. G. Bawendi, J. J. Macklin, J. K. Trautman, T. D. Harris, and L. E. Brus (1996). *Nature* **383**, (6603), 802.
21. L. Manna, E. Scher, and A. P. Alivisatos (2000). *J. Am. Chem. Soc.* **122**, 12700.
22. W. Wang, S. Banerjee, S. G. Jia, M. L. Steigerwald, and I. P. Herman (2007). *Chem. Mater.* **19**, 2573.
23. Z. A. Peng and X. G. Peng (2001). *J. Am. Chem. Soc.* **123**, (1), 183.
24. D. Wu, M. E. Kordesch, and P. G. V. Patten (2005). *Chem. Mater.* **17**, 6436.
25. V. Dzhanan, I. Lokteva, C. Himcinschi, X. Jin, J. Kolny-Olesiak, and D. R. Zahn (2011). *Nanoscale Res. Lett.* **6**, 79.
26. M. Epifani, E. Pellicer, J. Arbiol, N. Sergent, T. Pagnier, and J. R. Morante (2008). *Langmuir* **24**, (19), 11182.
27. X. Chen, A. C. S. Samia, Y. Lou, and C. Burda (2005). *J. Am. Chem. Soc.* **127**, 4372.
28. B. Mahler, N. Lequeux, and B. Dubertret (2009). *J. Am. Chem. Soc.* **132**, 953.
29. A. Morris-Cohen, M. T. Frederick, G. D. Lilly, E. A. McArthur, and E. A. Weiss (2010). *J. Phys. Chem. Lett.* **1**, 1078.
30. M. Mulvihill, S. Habas, I. Jen-La Plante, J. Wan, and T. Mokari (2010). *Chem. Mater.* **22**, 5251.
31. D. A. Navarro, S. Banerjee, D. S. Aga, and D. F. Watson (2010). *J. Colloid Interface Sci.* **348**, 119.
32. M. D. Regulacio and M. Y. Han (2010). *Acc. Chem. Res.* **43**, 621.
33. P. Zrazhevskiy, M. Sena, and X. Gao (2010). *Chem. Soc. Rev.* **39**, 4326.
34. S. Rosenthal, J. Chang, O. Kovtun, J. R. McBride, and I. D. Tomlinson (2011). *Chem. Biol.* **18**, 10.
35. K. Susumu, B. C. Mei, and H. Mattoussi (2009). *Nat. Protoc.* **4**, 424.
36. L. R. Becerra, C. B. Murray, G. G. Griffin, and M. G. Bawendi (1994). *J. Chem. Phys.* **100**, 3297.
37. J. E. B. Katarı, V. L. Colven, and A. P. Alivisatos (1994). *J. Phys. Chem.* **98**, 4109.
38. S. Sharma, Z. S. Pillai, and P. V. Kamat (2003). *J. Phys. Chem. B* **107**, 10088.
39. A. Haesselbarth, A. Eychemueller, and H. Weller (1993). *Chem. Phys. Lett.* **203**, 271.
40. N. A. Hill and K. B. Whaley (1994). *J. Chem. Phys.* **100**, (4), 2831.
41. V. I. Klimov, A. A. Mikhailovsky, D. W. McBranch, C. A. Leatherdale, and M. G. Bawendi (2000). *Phys. Rev. B* **61**, R13349.
42. R. G. Xie, U. Kolb, J. X. Li, T. Bashe, and A. Mews (2005). *J. Am. Chem. Soc.* **127**, 7480.
43. S. J. Clarke, C. A. Hollmann, F. A. Aldaye, and J. L. Nadeau (2008). *Bioconj. Chem.* **19**, 562.
44. M. A. Schreuder, J. R. McBride, A. D. Dukes III, J. A. Sammons, and S. J. Rosenthal (2009). *J. Phys. Chem. C* **113**, 8169.
45. A. Henglein (1993). *J. Phys. Chem.* **97**, 5457.
46. C. F. Landes, M. Braun, and M. A. El-Sayed (2001). *J. Phys. Chem. B* **105**, 10554.
47. B. P. Aryal and D. E. Benson (2006). *J. Am. Chem. Soc.* **128**, 15986.
48. J. G. Liang, S. S. Zhang, X. P. Ai, X. H. Ji, and Z. K. He (2005). *Spectrochim Acta A* **61**, 2974.
49. D. R. Baker and P. V. Kamat (2010). *Langmuir* **26**, (13), 11272.
50. M. A. Caldwell, A. E. Albers, S. C. Levy, T. E. Pick, B. E. Cohen, B. A. Helms, and D. J. Milliron (2011). *Chem. Commun.* **47**, 556.
51. Claridge, S., Castleman Jr, A., Khanna, S., Murray, C.B., Sen, A., Weiss, P.S.: Cluster-assembled materials. *Acs Nano* (2009).
52. P. D. Cozzoli, T. Pellegrino, and L. Manna (2006). *Chem. Soc. Rev.* **35**, 1195.
53. A. V. Malko, A. A. Mikhailovsky, M. A. Petruska, J. A. Hollingsworth, and V. I. Klimov (2004). *J. Phys. Chem. B* **108**, 5250.
54. V. M. Huxter and G. Scholes (2009). *J. Nanophoton.* **3**, (1), 032504. doi:10.1117/1.3276902.
55. A. M. Smith and S. Nie (2009). *Acc. Chem. Res.* **43**, 190.
56. D. V. Talapin, J. S. Lee, M. V. Kovalenko, and E. V. Shevchenko (2009). *Chem. Rev.* **110**, 389.
57. Y. Yin and A. P. Alivisatos (2004). *Nature* **437**, 664.
58. A. Wolcott, R. Fitzmorris, O. Muzaffery, and J. Z. Zhang (2010). *Chem. Mater.* **22**, 2814.
59. F. Wang, R. Tang, J. Kao, S. D. Dingman, and W. E. Buhro (2009). *J. Am. Chem. Soc.* **131**, 4983.
60. A. Cros-Gagneux, F. Delpech, C. Nayral, A. Cornejo, Y. Coppel, and B. Chaudret (2010). *J. Am. Chem. Soc.* **132**, 18147.
61. M. D. Donakowski, J. M. Godbe, R. Sknepnek, K. E. Knowles, M. O. de la Cruz, and E. A. Weiss (2010). *J. Phys. Chem. C* **114**, 22526.
62. A. M. Munro, I. Jen-La Plante, M. S. Ng, and D. S. Ginger (2007). *J. Phys. Chem. C* **111**, 6220.
63. I. Moreels, J. C. Martins, and Z. Hens (2006). *ChemPhysChem* **7**, 1028.

64. X. Ji, D. Copenhaver, C. Sichmeller, and X. Peng (2008). *J. Am. Chem. Soc.* **130**, 5726.
65. C. Bullen and P. Mulvaney (2006). *Langmuir* **22**, 3007.
66. B. Fritzinger, R. Capek, K. Lambert, J. C. Martins, and Z. Hens (2010). *J. Am. Chem. Soc.* **132**, 10195.
67. R. Gomes, A. Hassinen, A. Szczygiel, Q. Zhao, A. Vantomme, J. C. Martins, and Z. Hens (2011). *J. Phys. Chem. Lett.* **2**, 145.
68. Z. J. Jiang and D. F. Kelley (2010). *ACS Nano* **4**, 1561.
69. A. Dukes III, J. R. McBride, and S. J. Rosenthal (2010). *Chem. Mater.* **22**, 6402.
70. F. S. Riehle, R. Bienert, R. Thomann, G. A. Urban, and M. Kruger (2009). *Nano Lett* **9**, 514.
71. J. Huang, M. V. Kovalenko, and D. V. Talapin (2010). *J. Am. Chem. Soc.* **132**, 15866.
72. W. W. Yu, Y. A. Wang, and X. G. Peng (2003). *Chem. Mater.* **15**, (22), 4300.
73. J. T. Hu, L. W. Wang, L. S. Li, W. D. Yang, and A. P. Alivisatos (2002). *J. Phys. Chem. B* **106**, (10), 2447.
74. L. Manna, L. W. Wang, R. Cingolani, and A. P. Alivisatos (2005). *J. Phys. Chem. B* **109**, (13), 6183.
75. L. W. Wang, M. Califano, A. Zunger, and A. Franceschetti (2003). *Phys. Rev. Lett.* **91**, (5), 056404.
76. L. W. Wang and A. Zunger (1995). *Phys. Rev. B* **51**, (24), 17398.
77. L. W. Wang and A. Zunger (1996). *Phys. Rev. B* **53**, (15), 9579.
78. L. Pizzagalli, G. Galli, J. E. Klepeis, and F. Gygi (2001). *Phys. Rev. B* **63**, 16.
79. A. Puzder, A. J. Williamson, N. Zaitseva, G. Galli, G. Manna, and A. P. Alivisatos (2004). *Nano Lett.* **4**, (12), 2361.
80. A. Puzder, A. J. Williamson, F. Gygi, and G. Galli (2004). *Phys. Rev. Lett.* **92**, 217401.
81. A. Puzder, A. J. Williamson, F. Gygi, and G. Galli (2003). *Phys. Rev. Lett.* **91**, 037401.
82. K. Leung and K. B. Whaley (1999). *J. Chem. Phys.* **110**, (22), 11012.
83. H. Haug and S. W. Kock *Quantum Theory of the Optical and Electronic Properties of Semiconductors* (World Scientific, Singapore, 1993).
84. A. Zunger (2001). *Phys. Stat. Sol. (b)* **224**, 727.
85. V. S. Gurin (1994). *J. Phys.* **6**, (42), 8691.
86. J. Robles, O. Mayorga, T. Lee, and D. Diaz (1999). *Nanostruct. Mater.* **11**, 283.
87. K. Toth and T. A. Pakkanen (1993). *J. Comput. Chem.* **14**, 667.
88. P. Deglmann, R. Ahlrichs, and K. Tsereteli (2002). *J. Chem. Phys.* **116**, (4), 1585.
89. J. Frenzel, J. O. Joswig, P. Sarkar, G. Seifert, and M. Springborg (2005). *Eur. J. Inorg. Chem.* **36**, 3585.
90. D. Porezag, T. Frauenheim, T. Kohler, G. Seifert, and R. Kaschner (1995). *Phys. Rev. B* **51**, 12947.
91. T. Frauenheim, G. Seifert, M. Elstner, T. Niehaus, C. Kohler, M. Amkreutz, M. Sternberg, Z. Hajnal, A. Di Carlo, and S. Suhai (2002). *J. Phys.* **14**, 3015.
92. J. M. Matxain, J. E. Fowler, and J. M. Ugalde (2000). *Phys. Rev. A* **61**, 053201.
93. M. C. Tropicovsky and J. R. Chelikowsky (2001). *J. Chem. Phys.* **114**, (2), 943.
94. J. O. Joswig, M. Springborg, and G. Seifert (2000). *J. Phys. Chem. B* **104**, 2617.
95. T. Rabin, B. Hetényi, and B. Berne (1999). *J. Chem. Phys.* **110**, 5355.
96. J. R. Sachleben, V. Colvin, L. Emsley, E. W. Wooten, and A. P. Alivisatos (1998). *J. Phys. Chem. B* **102**, (50), 10117.
97. D. J. Milliron, A. P. Alivisatos, C. Pitois, C. Edder, and J. M. J. Frechet (2003). *Adv. Mater.* **15**, (1), 58.
98. S. Pokrant and K. B. Whaley (1999). *Eur. Phys. J. D* **6**, (2), 255.
99. G. W. Bryant and W. Jaskolski (2005). *J. Phys. Chem. B* **109**, 19650.
100. M. Korkusinski, O. Voznyy, and P. Hawrylak (2010). *Phys. Rev. B* **82**, 245304.
101. A. Franceschetti and A. Zunger (2000). *Appl. Phys. Lett.* **76**, (13), 1731.
102. P. C. Chen and K. B. Whaley (2004). *Phys. Rev. B* **70**, (4), 45311.
103. L. Wang (2009). *Energy Environ. Sci.* **2**, 944.
104. P. Yang, S. Tretiak, A. Masunov, and S. Ivanov (2008). *J. Chem. Phys.* **129**, 074709.
105. S. Y. Chung, S. Lee, C. Liu, and D. Neuhauser (2009). *J. Phys. Chem. B* **113**, 292.
106. H. Chou, C. Tseng, K. Pillai, B. Hwang, and L. Y. Chen (2010). *Nanoscale* **2**, 2679.
107. J. Y. Rempel, B. L. Trout, M. G. Bawendi, and K. F. Jensen (2006). *J. Phys. Chem. B* **110**, 18007.
108. H. Liu (2009). *J. Phys. Chem. C* **113**, 3116.
109. Y. B. Gu, K. Tan, and M. H. Lin (2010). *J. Mol. Struct.* **961**, 62.
110. M. Zanella, A. Z. Abbasi, A. K. Schaper, and W. J. Parak (2010). *J. Phys. Chem. C* **114**, 6205.

111. T. Inerbaev, A. Masunov, S. Khondaker, A. Dobrinescu, A. V. Plamada, and Y. Kawazoe (2009). *J. Chem. Phys.* **131**, 044106.
112. S. Kilina, S. Ivanov, and S. Tretiak (2009). *J. Am. Chem. Soc.* **131**, 7717.
113. H. Kim, S. Jang, S. Chung, S. Lee, Y. Lee, B. Kim, C. Liu, and D. Neuhauser (2009). *J. Phys. Chem. C* **114**, 471.
114. K. Knowles, D. Tice, E. A. McArthur, G. C. Solomon, and E. A. Weiss (2009). *J. Am. Chem. Soc.* **132**, 1041.
115. C. Liu, S. Chung, S. Lee, S. Weiss, and D. Neuhauser (2009). *J. Chem. Phys.* **131**, 174705.
116. J. B. Sambur, S. C. Riha, D. Choi, and B. A. Parkinson (2010). *Langmuir* **26**, 4839.
117. P. Schapotschnikow, B. Hommersom, and T. J. H. Vlugt (2009). *J. Phys. Chem. C* **113**, 12690.
118. K. Nguyen, P. N. Day, and R. Pachter (2010). *J. Phys. Chem. C* **114**, 16197.
119. G. Pilania, T. Sadowski, and R. Ramprasad (2009). *J. Phys. Chem. C* **113**, 1863.
120. I. Csik, S. P. Russo, and P. Mulvaney (2008). *J. Phys. Chem. C* **112**, 20413.
121. G. Neshet, L. Kronik, and J. Chelikowsky (2005). *Phys. Rev. B* **71**, 3.
122. J. Frenzel, J.-O. Joswig, and G. Seifert (2007). *J. Phys. Chem. C* **111**, 10761.
123. J. Schrier and L. W. Wang (2006). *J. Phys. Chem. B* **110**, 11982.
124. R. Jose, N. U. Zhanpeisov, H. Fukumura, Y. Baba, and M. Ishikawa (2006). *J. Am. Chem. Soc.* **128**, 629.
125. Frisch, M. J., G. W. Trucks, H. B. Schlegel et al., *Gaussian 03* (Gaussian Inc., Wallingford, CT, 2004).
126. Z. A. Peng and X. G. Peng (2002). *J. Am. Chem. Soc.* **124**, (13), 3343.
127. A. Kasuya, R. Sivamohan, Y. A. Barnakov, I. M. Dmitruk, T. Nirasawa, V. R. Romanyuk, V. Kumar, S. V. Mamykin, K. Tohji, B. Jeyadevan, K. Shinoda, T. Kudo, O. Terasaki, Z. Liu, R. V. Belosludov, V. Sundararajan, and Y. Kawazoe (2004). *Nat. Mater.* **3**, 99.